Supporting Information

Fabrication of carbon-based materials derived from a cobalt-based organic framework for enhancing photocatalytic degradation of dyes

Wan-Lin Ma,[a] Ya-Qian Zhang,[a*] Wen-Ze Li,[a*] Jing Li[a] and Jian Luan[a*]

[a] College of Science, Shenyang University of Chemical Technology, Shenyang, 110142, P. R. China

* *E-mails: zhangyaqian85@126.com; wzli@syuct.edu.cn; 2010044@stu.neu.edu.cn*

Table S1 Crystal data and structure refinement for **Co-MOF**.

Complex	**Co-MOF**
Empirical formula	$C_{49}H_{59}Co_3N_8O_{20}$
Formula weight	1256.83
Temperature/K	293.15
Crystal system	Monoclinic
Space group	*C*2/*c*
a/Å	34.033(4)
b/Å	20.515(2)
c/Å	7.8110(10)
α/°	90
β/°	95.204(4)
γ/°	90
Volume/Å^3	5431.1(11)
Z	4
ρ_{calc} g/cm^3	1.537
μ/mm^{-1}	0.99
F(000)	2600
Crystal size/mm^3	0.18 × 0.17 × 0.15
Radiation	MoKα (*λ* = 0.71073)
2*θ* range for data collection/°	4.642 to 50.052
Index ranges	-40 ≤ h ≤ 37, -24 ≤ k ≤ 24, -9 ≤ l ≤ 9
Reflections collected	33805
Independent reflections	4789 [R_{int} = 0.0554, R_{sigma} = 0.0345]
Data/restraints/parameters	4789/13/339
Goodness-of-fit on F^2	1.059
Final R indexes [I ≥ 2σ (I)]	R_1 = 0.0777, wR_2 = 0.2317
Final R indexes [all data]	R_1 = 0.1003, wR_2 = 0.2550

Table S2 Selected bond distances (Å) and angles (°) for **Co-MOF**.

Co1–O1	2.198(4)	Co2–O3#1	2.169(4)
Co1–O2	2.124(4)	Co2–O3#2	2.169(4)
Co1–O4	2.060(5)	Co2–O6	2.074(5)
Co1–N1	2.112(5)	Co2–O6#3	2.074(5)
Co1–N3#1	2.107(5)	Co2–N2	2.128(5)
Co1–C1	2.498(6)	Co2–N2#3	2.128(5)
Co1–O5	2.080(9)	Co2–C5#2	2.519(7)
O1–Co1–C1	30.52(16)	O3#1–Co2–C5#2	30.08(10)
O2–Co1–O1	60.77(14)	O3#2–Co2–C5#2	30.08(10)
O2–Co1–C1	30.27(17)	O6#3–Co2–O3#1	87.44(17)
O4–Co1–O1	87.85(18)	O6–Co2–O3#1	89.41(18)
O4–Co1–O2	89.8(2)	O6#3–Co2–O3#2	89.41(18)
O4–Co1–N1	90.22(19)	O6–Co2–O3#2	87.44(17)
O4–Co1–N3#1	91.3(2)	O6–Co2–O6#3	176.4(2)
O4–Co1–C1	88.0(2)	O6–Co2–N2	93.1(2)
O4–Co1–O5	177.4(4)	O6#3–Co2–N2#3	93.1(2)
N1–Co1–O1	161.97(16)	O6#3–Co2–N2	89.2(2)
N1–Co1–O2	101.32(18)	O6–Co2–N2#3	89.2(2)
N1–Co1–C1	131.51(19)	O6–Co2–C5#2	88.18(12)
N3#1–Co1–O1	98.74(16)	O6#3–Co2–C5#2	88.18(12)
N3#1–Co1–O2	159.42(18)	N2#3–Co2–O3#1	99.91(16)
N3#1–Co1–N1	99.22(19)	N2–Co2–O3#2	99.90(16)
N3#1–Co1–C1	129.25(19)	N2–Co2–O3#1	159.79(17)
O5–Co1–O1	94.5(5)	N2#3–Co2–O3#2	159.79(17)
O5–Co1–O2	92.2(4)	N2#3–Co2–N2	100.2(3)
O5–Co1–N1	87.8(5)	N2–Co2–C5#2	129.91(13)
O5–Co1–C1	94.6(4)	N2#3–Co2–C5#2	129.91(13)
O3#1–Co2–O3#2	60.2(2)		

Symmetry codes: #1 3/2 – *x*, 1/2 + *y*, 1/2 – *z*; #2 1/2 + *x*, 1/2 + *y*, 1 + *z*; #3 2 – *x*, + *y*, 3/2 –*z*.

Table S3 Quasi-first-order rate constant of photocatalytic degradation of **Co-MOF** and its derived carbon materials.

Material	Rare constant k (min^{-1})				
	MB	RhB	GV	MO	RB
Co-MOF	6.232	6.381	0.005	0.004	0.002
Co-C200	5.149	7.206	0.003	0.004	0.004
Co-C400	0.001	5.266	0.005	0.003	0.002
Co-C600	0.002	0.001	0.006	0.007	0.002
Co-C800	0.009	0.001	0.008	0.017	0.003
Co-C1000	0.009	0.002	0.015	0.014	0.003

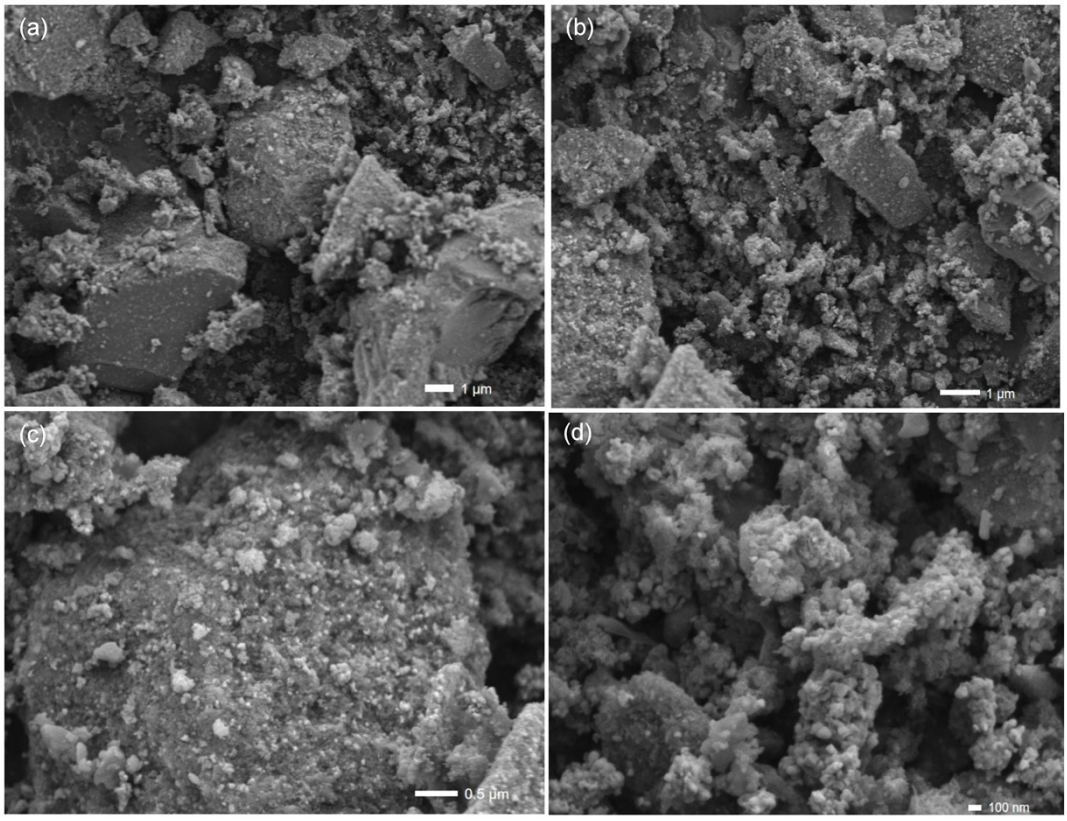

Fig. S1 SEM images of **Co-MOF**.

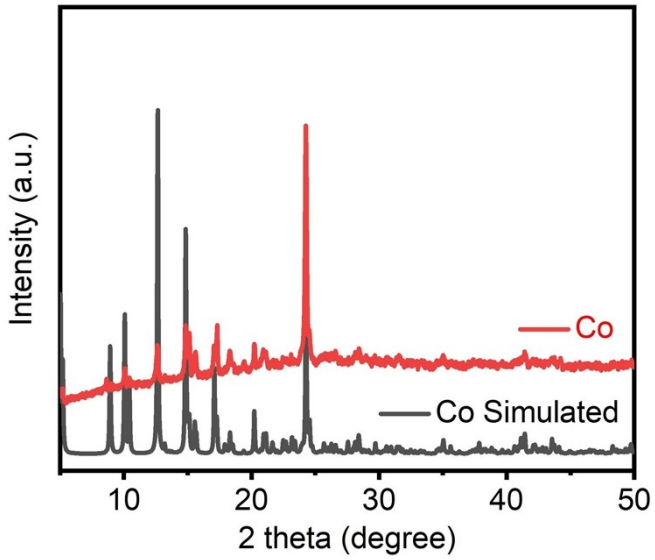

Fig. S2 The PXRD patterns of simulated and fresh sample of **Co-MOF**.

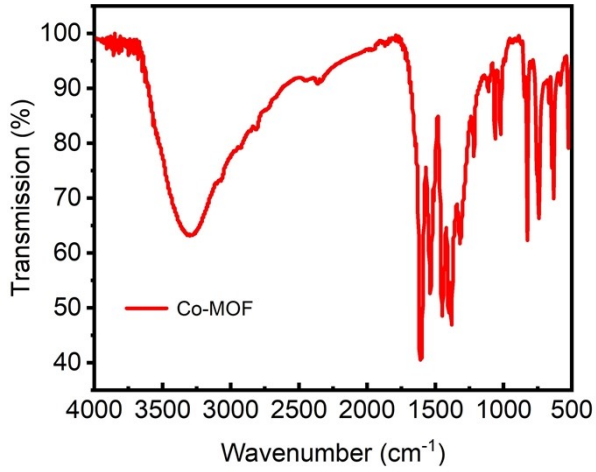

Fig. S3 The FTIR spectrum of **Co-MOF**.

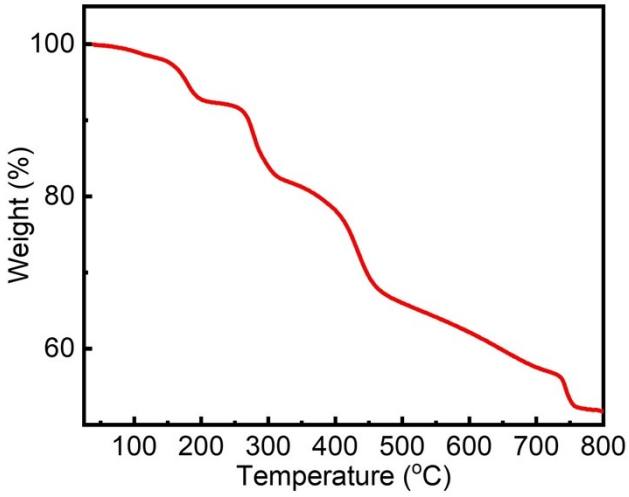

Fig. S4 The TG curve of **Co-MOF**.

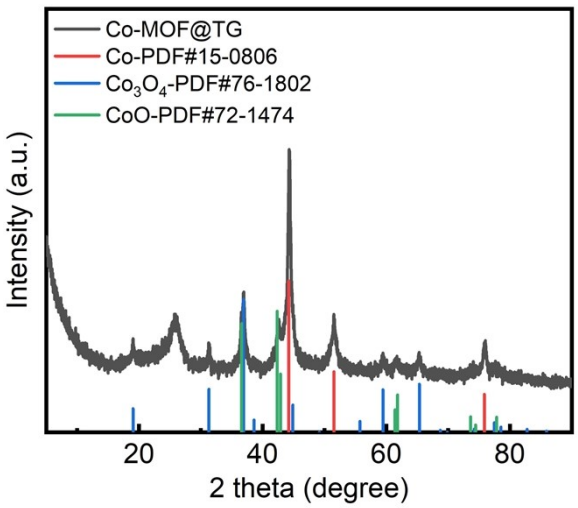

Fig. S5 PXRD pattern of TG residue of **Co-MOF**.

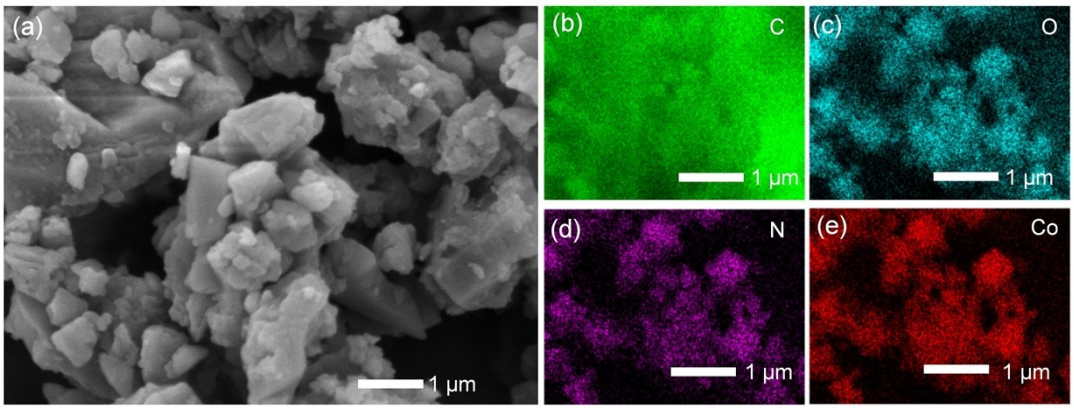

Fig. S6 Typical SEM (a) and EDX (b–e) images of **Co-C200** and the corresponding elemental maps of Co, N, C and O.

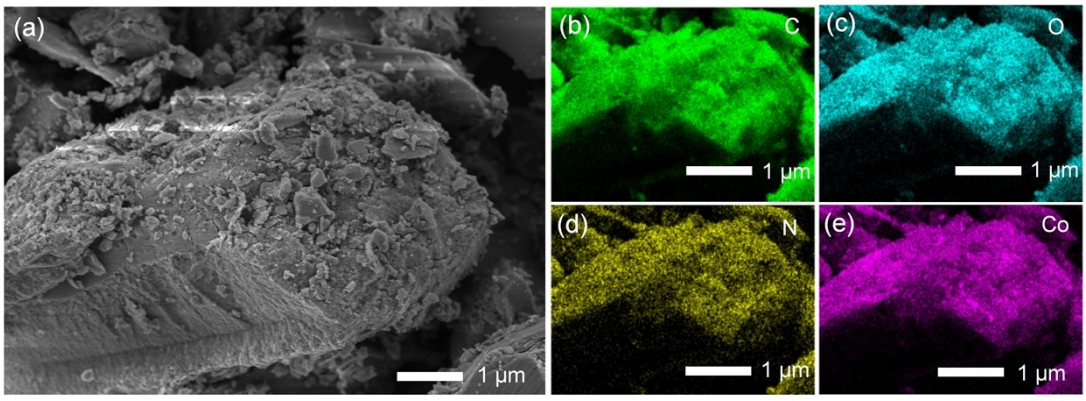

Fig. S7 Typical SEM (a) and EDX (b–e) images of **Co-C400** and the corresponding elemental maps of Co, N, C and O.

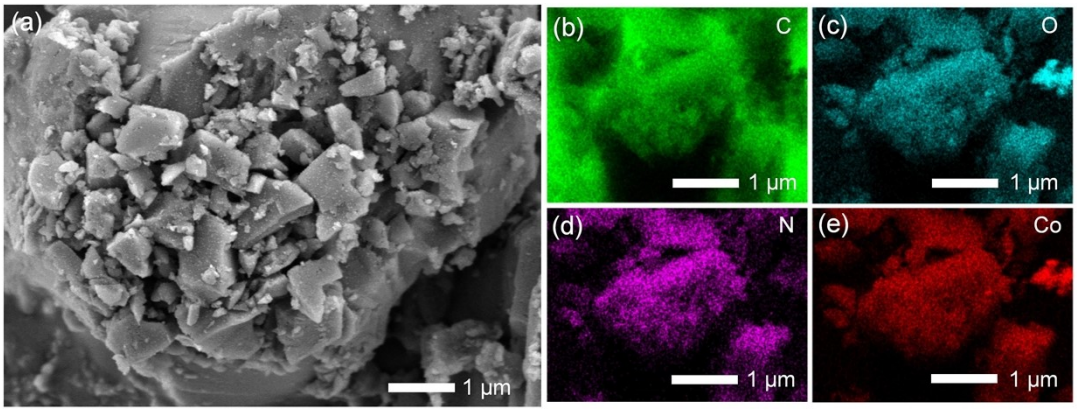

Fig. S8 Typical SEM (a) and EDX (b–e) images of **Co-C600** and the corresponding elemental maps of Co, N, C and O.

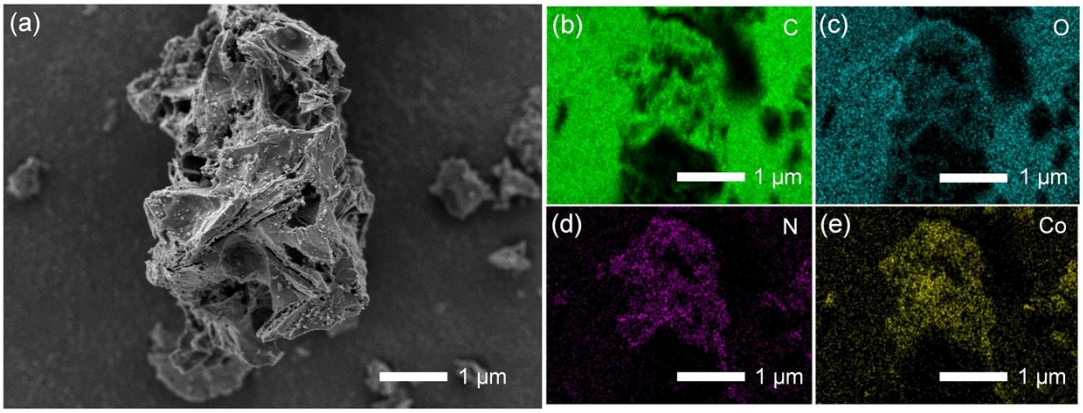

Fig. S9 Typical SEM (a) and EDX (b–e) images of **Co-C800** and the corresponding elemental maps of Co, N, C and O.

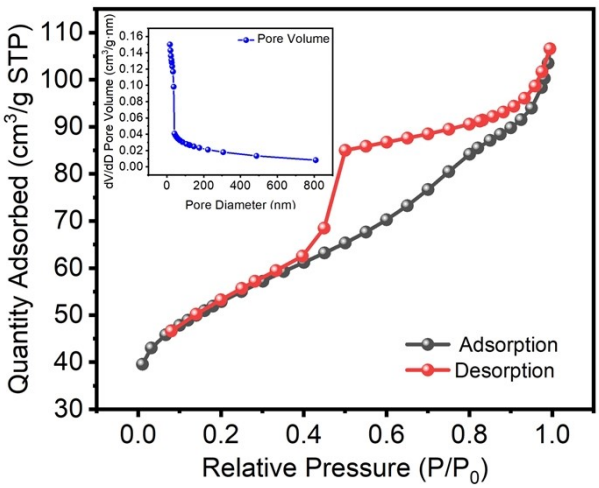

Fig. S10 Nitrogen adsorption and desorption isotherms (Insert: the pore size distribution) of **Co-C1000**.

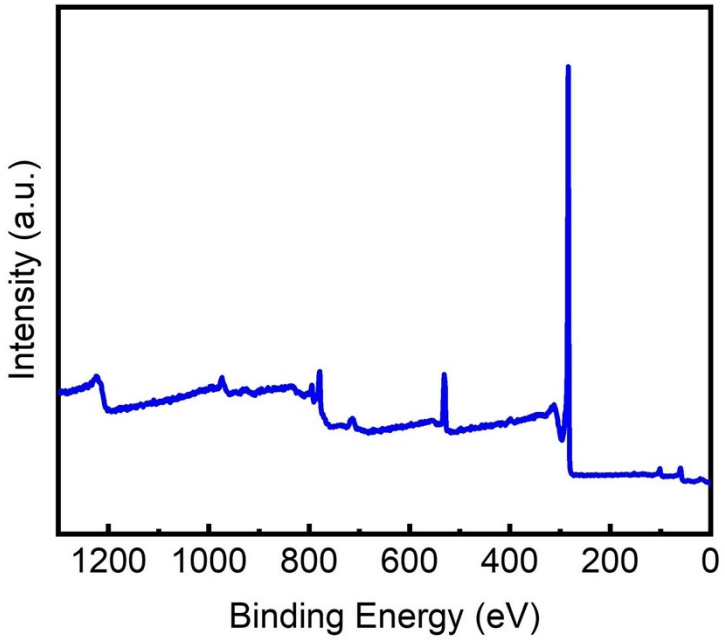

Fig. S11 XPS spectrum of **Co-C1000**.

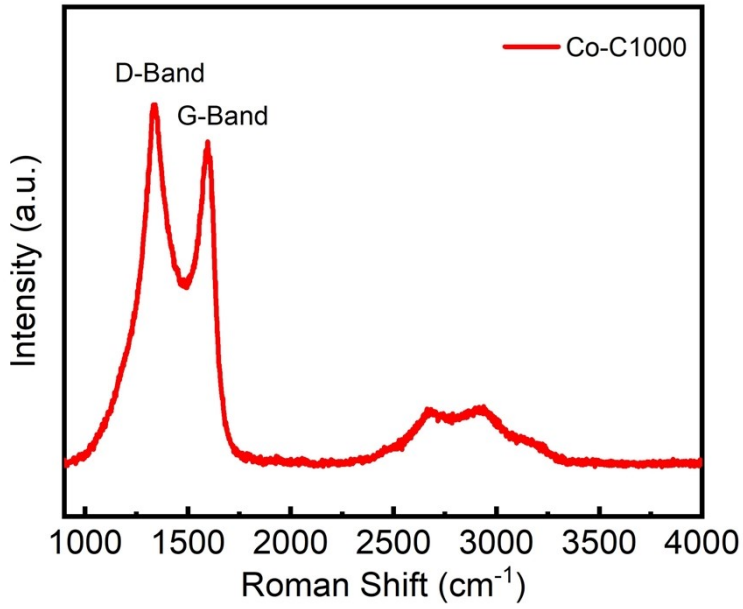

Fig. S12 Raman spectrum of **Co-C1000**.

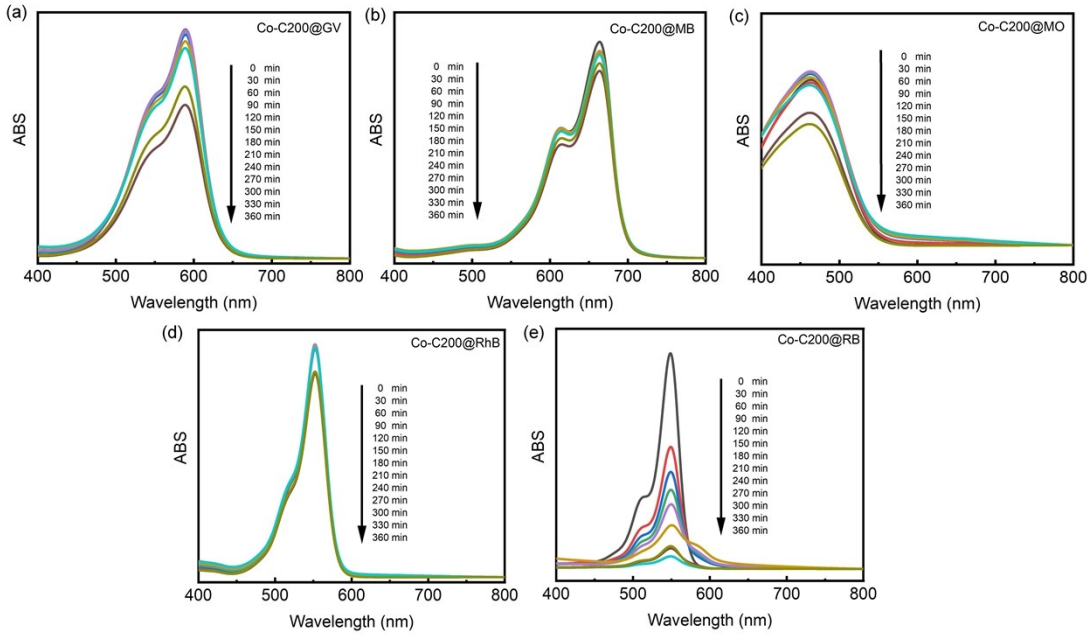

Fig. S13 UV-vis spectra of GV (a), MB (b), MO (c), RhB (d) and RB (e) solutions recorded with **Co-C200** after different degradation times.

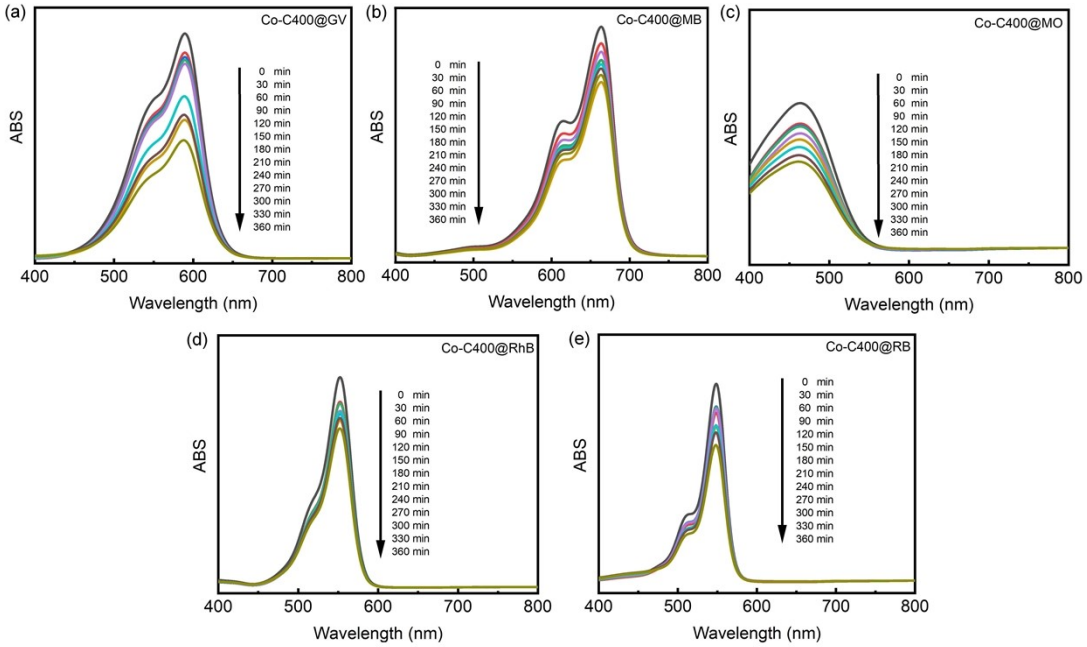

Fig. S14 UV-vis spectra of GV (a), MB (b), MO (c), RhB (d) and RB (e) solutions recorded with **Co-C400** after different degradation times.

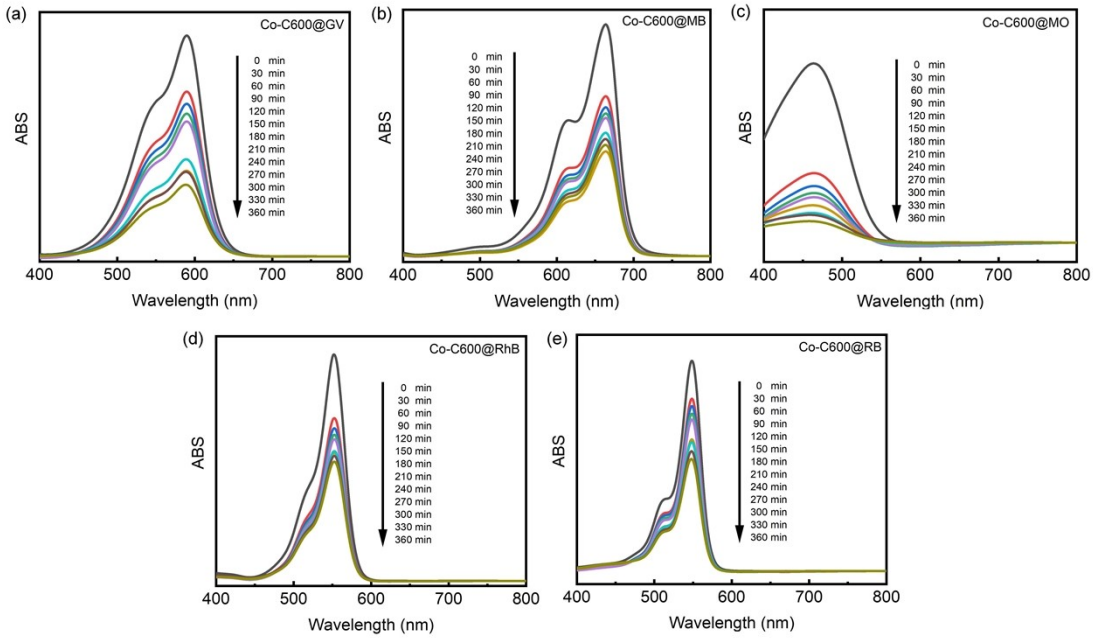

Fig. S15 UV-vis spectra of GV (a), MB (b), MO (c), RhB (d) and RB (e) solutions recorded with **Co-C600** after different degradation times.

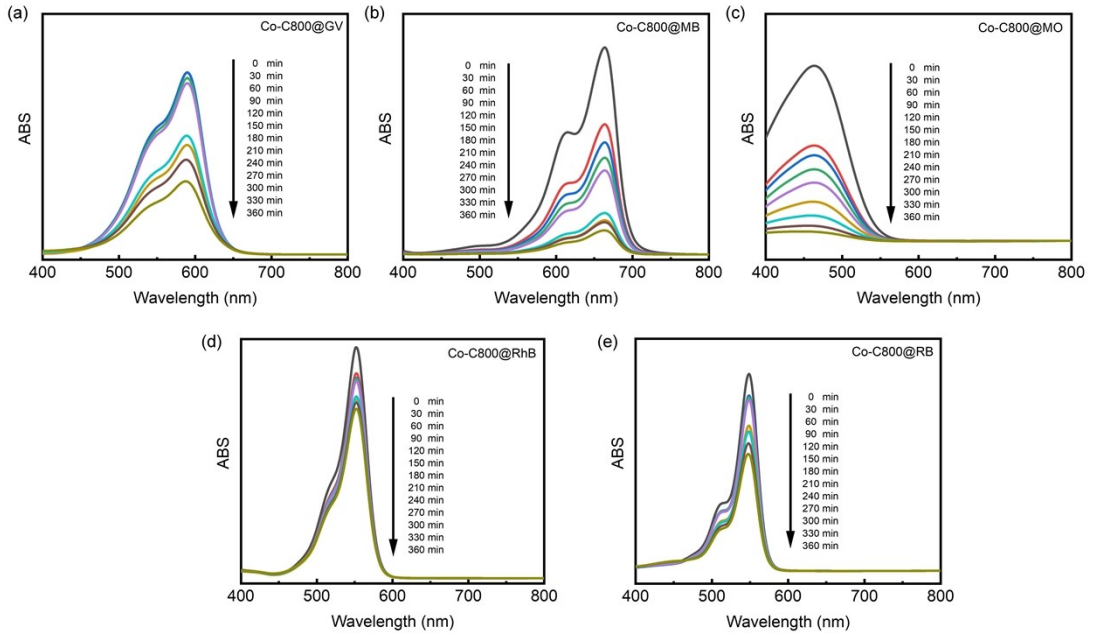

Fig. S16 UV-vis spectra of GV (a), MB (b), MO (c), RhB (d) and RB (e) solutions recorded with **Co-C800** after different degradation times.

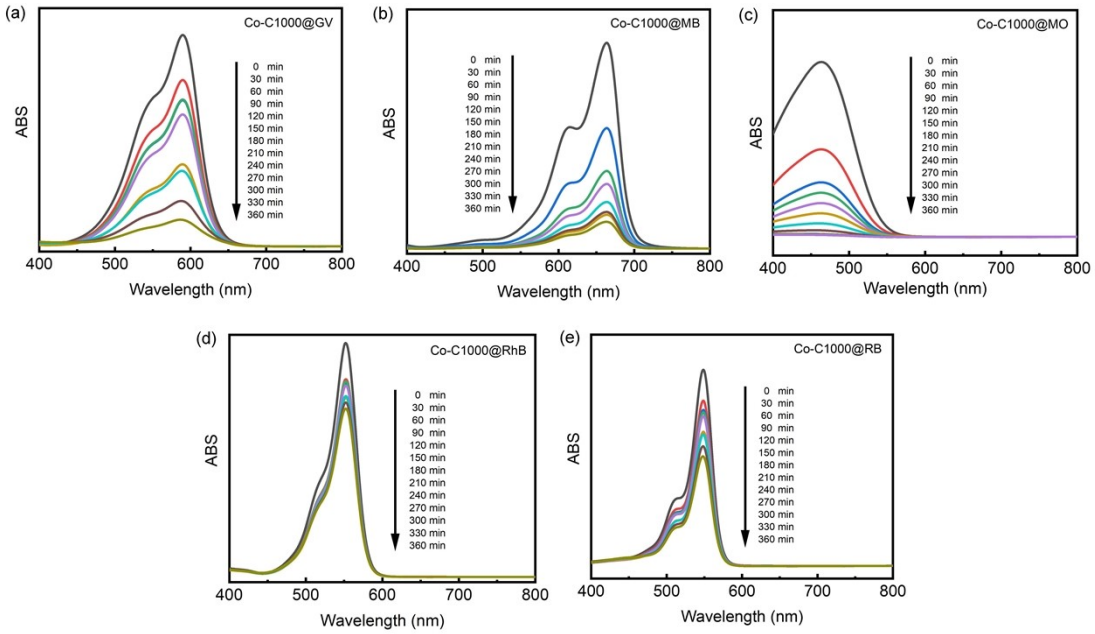

Fig. S17 UV-vis spectra of GV (a), MB (b), MO (c), RhB (d) and RB (e) solutions recorded with **Co-C1000** after different degradation times.

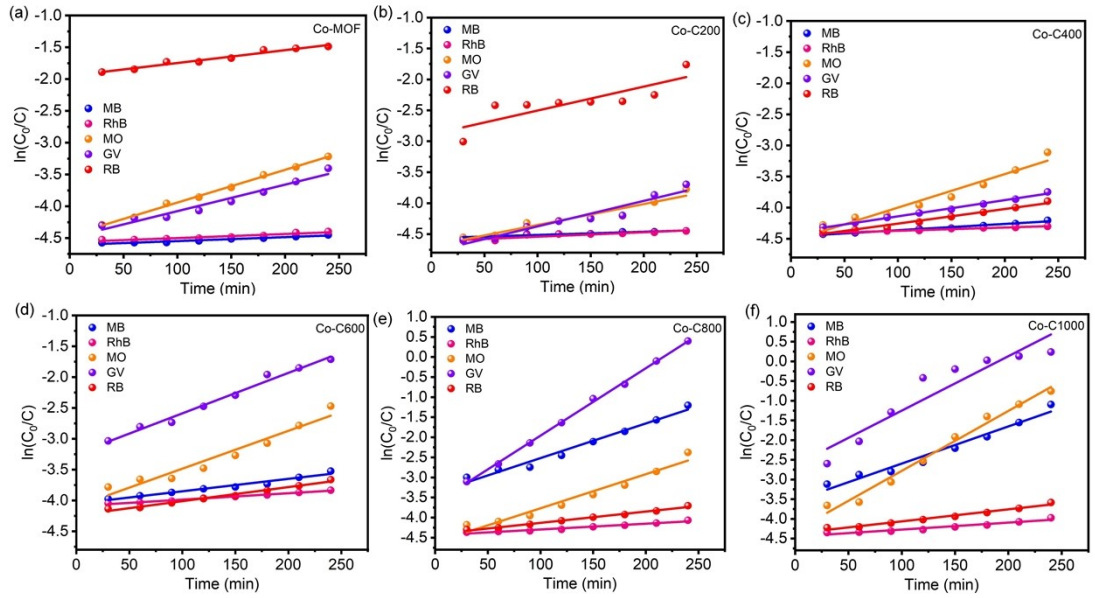

Fig. S18 Comparison of the rate constant k in the presence of **Co-MOF** and its derived carbon materials (evaluating that the reactions by the pseudo-first-order kinetic model).

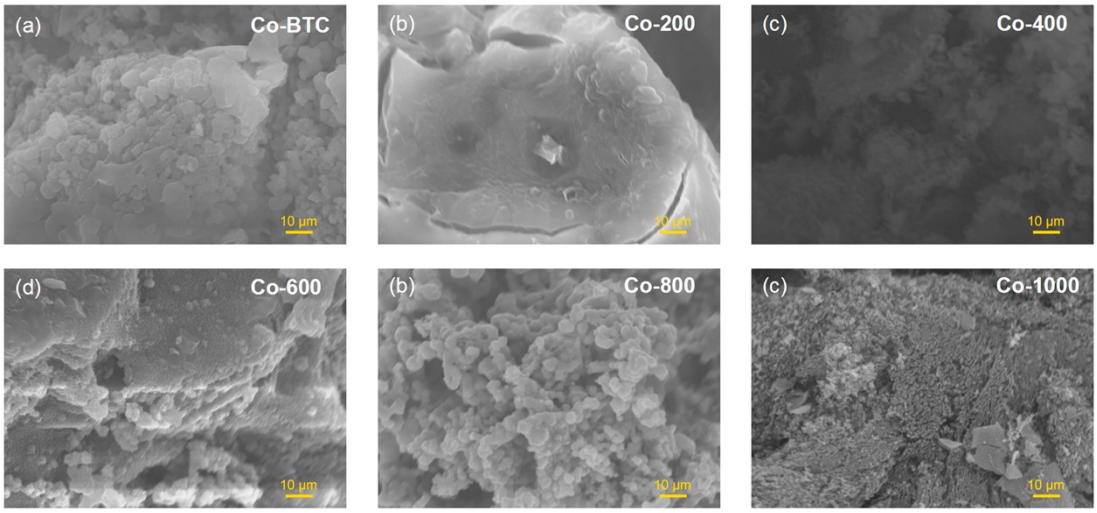

Fig. S19 Typical SEM images of **Co-BTC** (a), **Co-200** (b), **Co-400** (c), **Co-600** (d), **Co-800** (e), **Co-1000** (f).

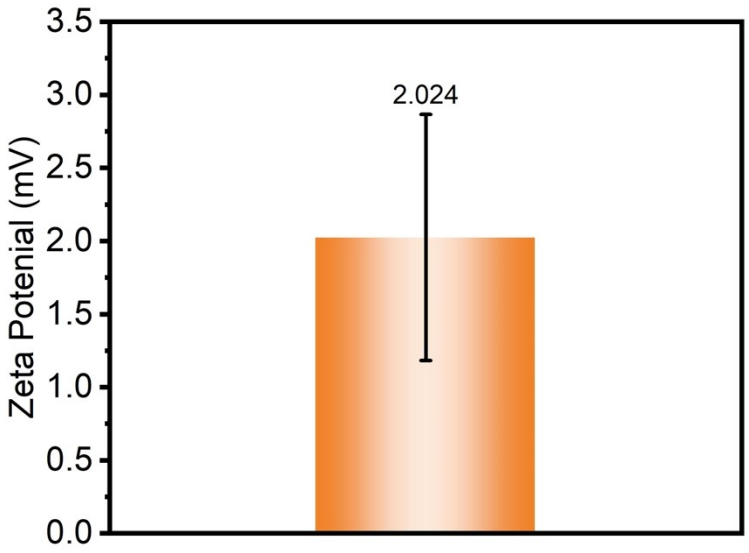

Fig. S20 Zeta potential of **Co-C1000**.